

Nearly conformal gauge theories in finite volume

Zoltan Fodor^a, Kieran Holland^b, Julius Kuti^{*c}, Dániel Nógrádi^c, Chris Schroeder^c

^a*Department of Physics, University of Wuppertal
Gaussstrasse 20, D-42119, Germany*

^b*Department of Physics, University of the Pacific
3601 Pacific Ave, Stockton CA 95211, USA*

^c*Department of Physics 0319, University of California, San Diego
9500 Gilman Drive, La Jolla, CA 92093, USA*

Abstract

We report new results on nearly conformal gauge theories with fermions in the fundamental representation of the SU(3) color gauge group as the number of fermion flavors is varied in the $N_f = 4 - 16$ range. To unambiguously identify the chirally broken phase below the conformal window we apply a comprehensive lattice tool set in finite volumes which includes the test of Goldstone pion dynamics, the spectrum of the fermion Dirac operator, and eigenvalue distributions of random matrix theory. We also discuss the theory inside the conformal window and present our first results on the running of the renormalized gauge coupling and the renormalization group beta function. The importance of understanding finite volume zero momentum gauge field dynamics inside the conformal window is illustrated. Staggered lattice fermions are used throughout the calculations.

Key words: lattice simulations, electroweak sector, technicolor, conformal

1. Introduction

The Large Hadron Collider will probe the mechanism of electroweak symmetry breaking. It is an intriguing possibility that new physics beyond the Standard Model might take the form of some new strongly-interacting gauge theory. In one scenario, the Higgs sector of the electroweak theory is replaced by a so-called technicolor theory, whose dynamics provides the required spontaneous symmetry breaking [1, 2, 3]. These models avoid the fine-tuning problem and may lead to a heavy composite Higgs particle on the TeV scale. Although attractive, the challenge is to extend a technicolor theory to include fermion mass generation, while satisfying the various constraints of electroweak phenomenology. This idea has lately been revived by new explorations of the multi-dimensional theory space of nearly conformal gauge theories [4, 5, 6, 7]. The terminology of *technicolor* in this report will refer in a generic sense to these investigations. Exploring the new technicolor ideas has to be based on nonperturbative studies which are only becoming feasible now with the advent of new lattice technologies.

Model building of a strongly interacting electroweak sector requires the knowledge of the phase diagram of nearly conformal gauge theories as the number of colors N_c , number of fermion flavors N_f , and the fermion representation R of the technicolor group are varied in theory space. For fixed N_c and R the theory is in the chirally broken phase for low N_f and asymptotic freedom is maintained with a negative β function. On the

other hand, if N_f is large enough, the β function is positive for all couplings, and the theory is trivial. If the regulator cut-off is removed, we are left with a free non-interacting continuum theory. There is some range of N_f for which the β function might have a non-trivial zero, an infrared fixed point, where the theory is in fact conformal [10, 11]. This method has been refined by estimating the critical value of N_f , above which spontaneous chiral symmetry breaking no longer occurs [12, 13, 14].

Interesting models require the theory to be very close to, but below, the conformal window, with a running coupling which is almost constant over a large energy range [15, 16, 17, 18, 19]. The nonperturbative knowledge of the critical N_f^{crit} separating the two phases is essential and this has generated much interest and many new lattice studies [20, 21, 22, 23, 24, 25, 26, 27, 28, 29, 30, 31, 32, 33, 34, 35, 36, 37, 38, 39, 40, 41, 42, 43, 44, 45, 46].

Our goal to unambiguously identify the chirally broken phase below the conformal window requires the application and testing of a comprehensive lattice tool set in finite volumes which includes the test of Goldstone pion dynamics, the spectrum of the fermion Dirac operator, and eigenvalue distributions of Random Matrix Theory (RMT). Inside the conformal window we investigate the running coupling and the β function. We report new results at $N_f = 4, 8, 9, 12, 16$ for fermions in the fundamental representation of the SU(3) technicolor gauge group. We find $N_f = 4, 8, 9$ to be in the chirally broken phase and $N_f = 16$ is consistent with the expected location inside the conformal window. To resolve the $N_f = 12$ phase from our simulations will require further analysis.

*Corresponding author

Email address: jkuti@ucsd.edu (Julius Kuti)

2. Chiral symmetry breaking below the conformal window

We will identify in lattice simulations the chirally broken phases with $N_f = 4, 8, 9$ flavors of staggered fermions in the fundamental $SU(3)$ color representation using finite volume analysis. The staggered fermions are deployed with a special 6-step exponential (stout) smearing procedure [47] in the lattice action to reduce well-known cutoff effects with taste breaking in the Goldstone spectrum. The presence of taste breaking requires a brief explanation of how staggered chiral perturbation theory is applied in our analysis. The important work of Lee, Sharpe, Aubin and Bernard [48, 49, 50] is closely followed in the discussion.

2.1. Staggered chiral perturbation theory

Starting with the $N_f = 4$ example [48], the spontaneous breakdown of $SU(4)_L \times SU(4)_R$ to vector $SU(4)$ gives rise to 15 Goldstone modes, described by fields ϕ_i . These can be organized into an $SU(4)$ matrix

$$\Sigma(x) = \exp\left(i\frac{\phi}{\sqrt{2}F}\right), \quad \phi = \sum_{a=1}^{15} \phi_a T_a, \quad (1)$$

where F is the Goldstone decay constant in the chiral limit and the normalization $T_a = \{\xi_\mu, i\xi_{\mu 5}, i\xi_{\mu\nu}, \xi_5\}$ is used for the flavor generators. The leading order chiral Lagrangian is given by

$$\mathcal{L}_\chi^{(4)} = \frac{F^2}{4} \text{Tr}(\partial_\mu \Sigma \partial_\mu \Sigma^\dagger) - \frac{1}{2} B m_q F^2 \text{Tr}(\Sigma + \Sigma^\dagger), \quad (2)$$

with the fundamental parameters F and B measured on the technicolor scale Λ_{TC} which replaced Λ_{QCD} in the new theory. Expanding the chiral Lagrangian in powers of ϕ one finds 15 degenerate pions with masses given by

$$M_\pi^2 = 2Bm_q \left[1 + O(m_q/\Lambda_{\text{TC}})\right]. \quad (3)$$

The leading order term is the tree-level result, while the corrections come from loop diagrams and from higher order terms in the chiral Lagrangian. The addition of $a^2 \mathcal{L}_\chi^{(6)}$ breaks chiral symmetry and lifts the degeneracy of the Goldstone pions. Correction terms are added to Eq. (3) which becomes

$$M_\pi^2 = C(T_a) \cdot a^2 \Lambda_{\text{TC}}^4 + 2Bm_q \left[1 + O(m_q/\Lambda_{\text{TC}}) + O(a^2 \Lambda_{\text{TC}}^2)\right] \quad (4)$$

where the representation dependent $C(T_a)$ is a constant of order unity. Contributions proportional to a^2 are due to $\mathcal{L}_\chi^{(6)}$, and lead to massive Goldstone pions even in the $m_q \rightarrow 0$ chiral limit. The only exception is the pion with flavor ξ_5 which remains massless because the $U(1)_A$ symmetry is protected.

Lee and Sharpe observe that the part of $\mathcal{L}_\chi^{(6)}$ without derivatives, defining the potential $\mathcal{V}_\chi^{(6)}$, is invariant under flavor $SO(4)$ transformations and gives rise to the a^2 term in M_π^2 . Terms in $\mathcal{L}_\chi^{(6)}$ involving derivatives break $SO(4)$ further down to the lattice symmetry group and give rise to non-leading terms propor-

tional to $a^2 m$ and a^4 . The taste breaking potential is given by

$$\begin{aligned} -\mathcal{V}_\chi^{(6)} &= C_1 \text{Tr}(\xi_5 \Sigma \xi_5 \Sigma^\dagger) \\ &+ C_2 \frac{1}{2} \left[\text{Tr}(\Sigma^2) - \text{Tr}(\xi_5 \Sigma \xi_5 \Sigma) + h.c. \right] \\ &+ C_3 \frac{1}{2} \sum_\nu \left[\text{Tr}(\xi_\nu \Sigma \xi_\nu \Sigma) + h.c. \right] \\ &+ C_4 \frac{1}{2} \sum_\nu \left[\text{Tr}(\xi_{\nu 5} \Sigma \xi_{\nu 5} \Sigma) + h.c. \right] \\ &+ C_5 \frac{1}{2} \sum_\nu \left[\text{Tr}(\xi_\nu \Sigma \xi_\nu \Sigma^\dagger) - \text{Tr}(\xi_{\nu 5} \Sigma \xi_{\nu 5} \Sigma^\dagger) \right] \\ &+ C_6 \sum_{\mu < \nu} \text{Tr}(\xi_{\mu\nu} \Sigma \xi_{\mu\nu} \Sigma^\dagger). \end{aligned} \quad (5)$$

The six unknown coefficients C_i are all of size Λ_{TC}^6 .

In the continuum, the pions form a 15-plet of flavor $SU(4)$, and are degenerate. On the lattice, states are classified by the symmetries of the transfer matrix and the Goldstone pions fall into 7 irreducible representations: four 3-dimensional representations with flavors ξ_i , ξ_{i5} , ξ_{ij} and ξ_{i4} , and three 1-dimensional representations with flavors ξ_4 , ξ_{45} and ξ_5 .

Close to both the chiral and continuum limits, the pion masses are given by

$$M_\pi(T_a)^2 = 2Bm_q + a^2 \Delta(T_a) + O(a^2 m_q) + O(a^4), \quad (6)$$

with $\Delta(T_a) \sim \Lambda_{\text{TC}}^4$ arising from $\mathcal{V}_\chi^{(6)}$. Since $\mathcal{V}_\chi^{(6)}$ respects flavor $SO(4)$, the 15 Goldstone pions fall into $SO(4)$ representations:

$$\Delta(\xi_5) = 0, \quad (7)$$

$$\Delta(\xi_\mu) = \frac{8}{F^2} (C_1 + C_2 + C_3 + 3C_4 + C_5 + 3C_6), \quad (8)$$

$$\Delta(\xi_{\mu 5}) = \frac{8}{F^2} (C_1 + C_2 + 3C_3 + C_4 - C_5 + 3C_6), \quad (9)$$

$$\Delta(\xi_{\mu\nu}) = \frac{8}{F^2} (2C_3 + 2C_4 + 4C_6). \quad (10)$$

In the chiral limit at finite lattice spacing the lattice irreducible representations with flavors ξ_i and ξ_4 are degenerate, those with flavors ξ_{i5} and ξ_{45} , and those with flavors ξ_{ij} and ξ_{i4} are degenerate as well. No predictions can be made for the ordering or splittings of the mass shifts. We also cannot predict the *sign* of the shifts, although our simulations indicate that they are all positive with the exponentially smeared staggered action we use. This makes the existence of an Aoki phase [48] unlikely.

The method of [48] has been generalized in a nontrivial way to the $N_f > 4$ case [49, 50] which we adopted in our calculations with help from Bernard and Sharpe. The procedure cannot be reviewed here but it will be used in the interpretation of our $N_f = 8$ simulations.

2.2. Finite volume analysis in the p-regime

Three different regimes can be selected in simulations to identify the chirally broken phase from finite volume spectra and correlators. For a lattice size $L_s^3 \times L_t$ in euclidean space and in the limit $L_t \gg L_s$, the conditions $F_\pi L_s > 1$ and $M_\pi L_s > 1$ select the p-regime, in analogy with low momentum counting [51, 52].

For arbitrary N_f , in the continuum and in infinite volume, the one-loop chiral corrections to M_π and F_π of the degenerate Goldstone pions are given by

$$M_\pi^2 = M^2 \left[1 - \frac{M^2}{8\pi^2 N_f F^2} \ln\left(\frac{\Lambda_3}{M}\right) \right], \quad (11)$$

$$F_\pi = F \left[1 + \frac{N_f M^2}{16\pi^2 F^2} \ln\left(\frac{\Lambda_4}{M}\right) \right], \quad (12)$$

where $M^2 = 2B \cdot m_q$ and $F, B, \Lambda_3, \Lambda_4$ are four fundamental parameters of the chiral Lagrangian, and the small quark mass m_q explicitly breaks the symmetry [53]. The chiral parameters F, B appear in the leading part of the Lagrangian in Eq. (2), while Λ_3, Λ_4 enter in next order. There is the well-known GMOR relation $\Sigma_{cond} = BF^2$ in the $m_q \rightarrow 0$ limit for the chiral condensate per unit flavor [54]. It is important to note that the one-loop correction to the pion coupling constant F_π is enhanced by a factor N_f^2 compared to M_π^2 . The chiral expansion for large N_f will break down for F_π much faster for a given M_π/F_π ratio.

The finite volume corrections to M_π and F_π are given in the p-regime by

$$M_\pi(L_s, \eta) = M_\pi \left[1 + \frac{1}{2N_f} \frac{M^2}{16\pi^2 F^2} \cdot \tilde{g}_1(\lambda, \eta) \right], \quad (13)$$

$$F_\pi(L_s, \eta) = F_\pi \left[1 - \frac{N_f}{2} \frac{M^2}{16\pi^2 F^2} \cdot \tilde{g}_1(\lambda, \eta) \right], \quad (14)$$

where $\tilde{g}_1(\lambda, \eta)$ describes the finite volume corrections with $\lambda = M \cdot L_s$ and aspect ratio $\eta = L_t/L_s$. The form of $\tilde{g}_1(\lambda, \eta)$ is a complicated infinite sum which contains Bessel functions and requires numerical evaluation [52]. Eqs. (11-14) provide the foundation of the p-regime fits in our simulations.

2.3. δ -regime and ϵ -regime

At fixed L_s and in cylindrical geometry $L_t/L_s \gg 1$, a crossover occurs from the p-regime to the δ -regime when $m_q \rightarrow 0$, as shown in Fig. 1. The dynamics is dominated by the rotator states of the chiral condensate in this limit [55] which is characterized by the conditions $FL_s > 1$ and $ML_s \ll 1$. The densely spaced rotator spectrum scales with gaps of the order $\sim 1/F^2 L_s^3$, and at $m_q = 0$ the chiral symmetry is apparently restored. However, the rotator spectrum, even at $m_q = 0$ in the finite volume, will signal that the infinite system is in the chirally broken phase for the particular parameter set of the Lagrangian. This is often misunderstood in the interpretation of lattice simulations. Measuring finite energy levels with pion quantum numbers at fixed L_s in the $m_q \rightarrow 0$ limit is not a signal for chiral symmetry restoration of the infinite system [36].

If $L_t \sim L_s$ under the conditions $FL_s > 1$ and $ML_s \ll 1$, the system will be driven into the ϵ -regime which can be viewed as the high temperature limit of the δ -regime quantum rotator. Although the δ -regime and ϵ -regime have an overlapping region, there is an important difference in their dynamics. In the δ -regime of the quantum rotator, the zero spatial momentum of the pion field $U(x)$ dominates with time-dependent quantum dynamics. The ϵ -regime is dominated by the four-dimensional zero momentum mode of the chiral Lagrangian.

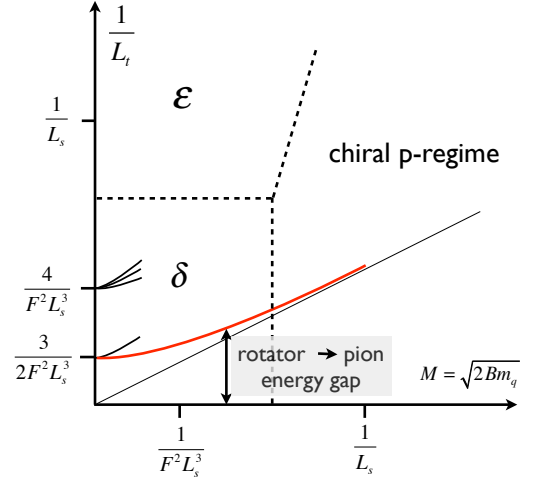


Figure 1: Schematic plot of the regions in which the three low energy chiral expansions are valid. The vertical axis shows the finite temperature scale (euclidean time in the path integral) which probes the rotator dynamics of the δ -regime and the ϵ -regime. The first two low lying rotator levels are also shown on the vertical axis for the simple case of $N_f = 2$. The fourfold degenerate lowest rotator excitation at $m_q = 0$ will split into an isotriplet state (lowest energy level), which evolves into the p-regime pion as m_q increases, and into an isosinglet state representing a multi-pion state in the p-regime. Higher rotator excitations have similar interpretations.

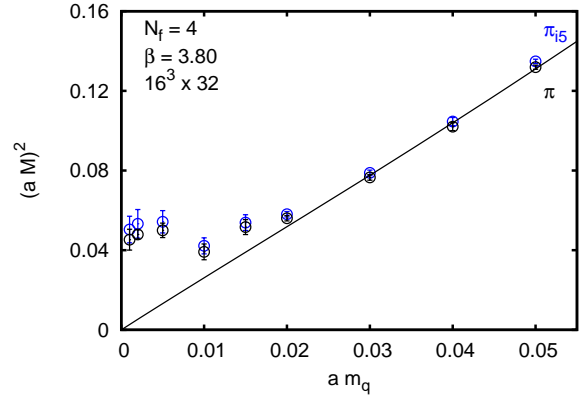


Figure 2: The crossover from the p-regime to the δ -regime is shown for the π and π_{i5} states at $N_f = 4$.

We report simulation results of all three regimes in the chirally broken phase of the technicolor models we investigate. The analysis of the three regimes complement each other and provide cross-checks for the correct identification of the phases. First, we will probe Eqs.(11-14) in the p-regime, and follow with the study of Dirac spectra and RMT eigenvalue distributions in the ϵ -regime. The spectrum in the δ -regime is used as a signal to monitor p-regime spectra as m_q decreases. Fig. 2 is an illustrative example for this crossover in our simulations.

3. Simulations results in the p-regime

The tree level improved Symanzik gauge action was used in our simulations. The link variables in the staggered fermion

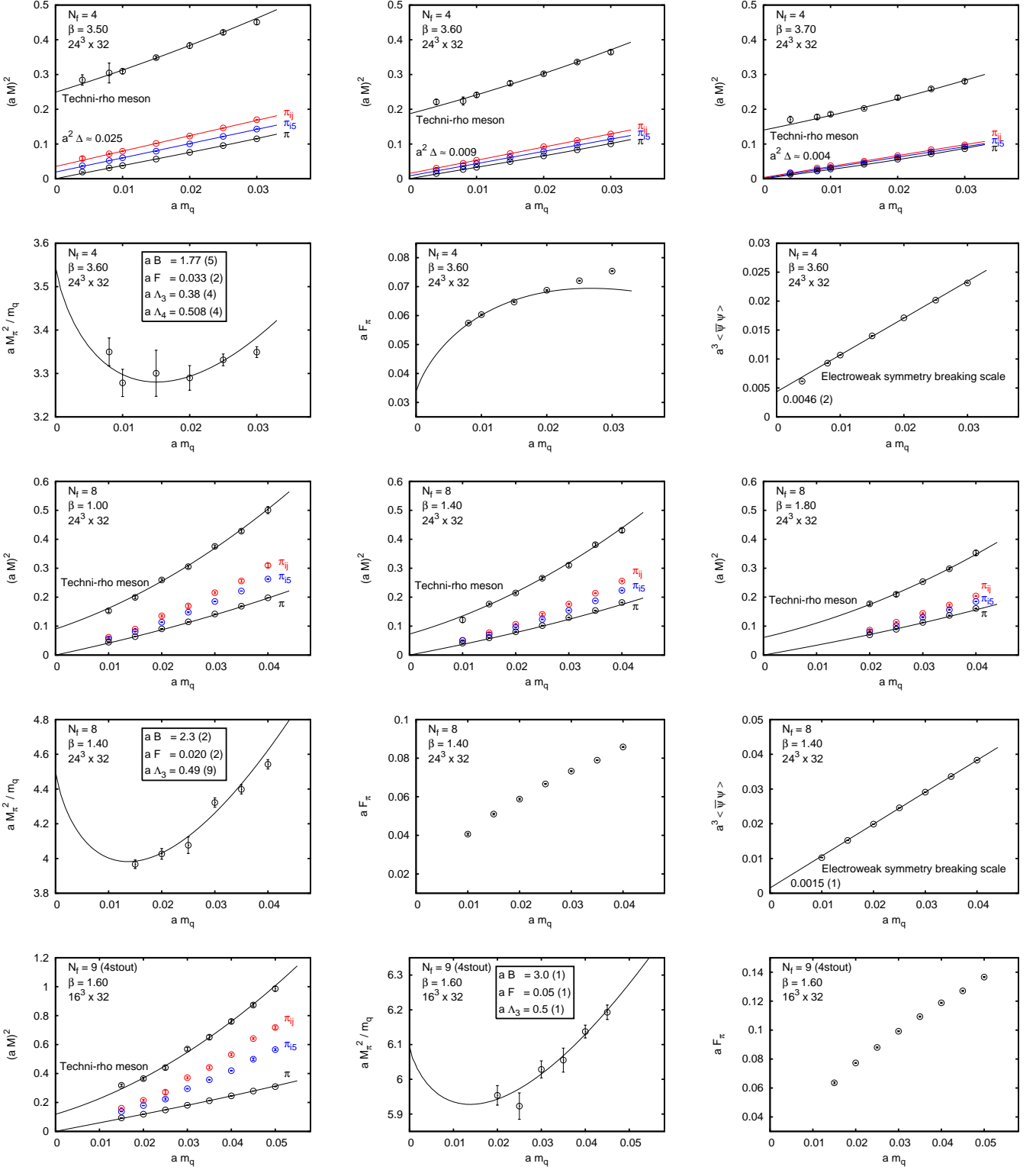


Figure 3: The first two rows of the composite figure show $N_f = 4$ simulation results in the p-regime. The first row depicts the collapsing pion spectrum and the techni-rho as the continuum limit is approached. The second row shows the chiral fits to M_π^2/m_q and F_π based on Eqs. (11-14). The range $m_q = 0.008 - 0.025$ is used in the fitting procedure. The approximately linear behavior of the chiral condensate $\langle \bar{\psi}\psi \rangle$ is also shown in the second row. The third and fourth rows summarize the simulation results for $N_f = 8$. The third row shows the collapsing pion spectrum and the techni-rho as the continuum limit is approached. The chiral fit to M_π^2/m_q is shown based on Eq. (11) only since the F_π data points are outside the convergence range of the chiral expansion. The range $m_q = 0.015 - 0.035$ is used in the fitting procedure. The fifth row illustrates our first simulation results for $N_f = 9$. It shows the split pion spectrum, chiral fit to M_π^2/m_q and the F_π data points are outside the convergence range of the chiral expansion. The range $m_q = 0.02 - 0.04$ is used in the fitting procedure.

matrix were exponentially smeared with six stout steps at $N_f = 4, 8$ and four stout steps at $N_f = 9$. The RHMC algorithm was deployed in all runs but rooting of the fermion determinant only affected the $N_f = 9$ simulations. The results shown in Fig. 3 are from the p-regime of the chirally broken phase with the conditions $M_\pi \cdot L_s \gg 1$ and $F_\pi \cdot L \sim 1$ when the chiral condensate begins to follow the expected behavior of infinite volume chiral perturbation theory from Eqs. (11,12) with calculable finite volume corrections from Eqs. (13,14).

The $N_f = 4$ simulations work in the p-regime as expected. The pion spectrum is clearly separated from the technicolor scale of the ρ -meson whose quadratic fit is just to guide the eye. Moving towards the continuum limit with increasing $\beta = 6/g^2$, we see the split pion spectrum collapsing onto the true Goldstone pion. The true Goldstone pion and two additional split pion states are shown. Δ is the measure of the small quadratic pion mass splittings in lattice units. Their origin was discussed in Section 2 in Eqs. (7-10). The spectrum is parallel and the gaps appear to be equally spaced consistent with the earlier observation in QCD where the C_4 term seems to dominate taste breaking accounting for the equally spaced pion levels [48]. The simultaneous chiral fit of M_π^2/m_q and F_π based on Eqs. (11-14) works when the chiral loop term corrects the tree level value of $M_\pi^2/m_q = 2B$. This is a chirally broken phase and the picture holds in the $m_q \rightarrow 0$ limit. The fit to determine the $N_f = 4$ chiral condensate for $m_q = 0$ is shown in the second row on the right. It sets the scale of electroweak symmetry breaking in the Higgs mechanism.

As we move to the $N_f = 8$ p-regime simulations summarized in the third and fourth rows of Fig. 3 we observe the weakening of the chiral condensate and increased difficulties in passing the chiral tests. The pion spectrum is still clearly separated from the technicolor scale of the ρ -meson. Moving towards the continuum limit with increasing $\beta = 6/g^2$, we see the split pion spectrum collapsing toward the true Goldstone pion with a new distinguished feature. The true Goldstone pion and two additional split pion states are shown with different slopes as m_q increases. Towards $m_q = 0$ the pion spectrum is collapsed at fixed gauge coupling, indicating that the effects of leading order taste breaking operators, the generalization of those from $N_f = 4$ to $N_f = 8$ as discussed in Section 2, are smaller than at $N_f = 4$ in the explored coupling constant range. This is somewhat unexpected and unexplained. Next to leading order taste breaking operators are responsible for the spread of the slopes and they seem to dominate. They were identified in Eq. (6) as the last two terms. It is reassuring to see that this structure is collapsing as we move toward the continuum limit. We analyzed this pattern within staggered perturbation theory in its generalized form beyond four flavors [49, 50]. The simultaneous chiral fit of M_π^2/m_q and F_π based on Eqs. (11-14) cannot be done at $N_f = 8$ within the reach of the largest lattice sizes we deploy since the value of aF is too small even at $L=24$ for coupling constants where taste breaking drops to an acceptable level. The chiral fit to M_π^2/m_q is shown based on Eq. (11) only since the F_π data points are outside the convergence range of the chiral expansion. We would need much bigger lattices to drop further down in the p-regime with m_q to the region where

the simultaneous fit could be made. It is also important to note that the chiral condensate is very small in the $m_q \rightarrow 0$ limit in the region where taste breaking is not large. This is shown in row four of Fig. 3 on the right side.

The $N_f = 9$ p-regime simulations are summarized in the fifth row of Fig. 3 where we observe the continued weakening of the chiral condensate and the increased difficulties in passing the chiral tests. The pion spectrum is still clearly separated from the technicolor scale of the ρ -meson. Moving towards the continuum limit to see the split pion spectrum collapsing toward the true Goldstone pion is increasingly difficult. The true Goldstone pion and two additional split pion states are shown again with different slopes as m_q increases. Forcing the collapse of the split pion spectrum will require larger lattices with smaller gauge couplings. The trends and the underlying explanation is very similar to the $N_f = 8$ case. The chiral fit to M_π^2/m_q is shown based on Eq. (11) only since the F_π data points are outside the convergence range of the chiral expansion.

In summary, we have shown that according to p-regime tests the $N_f = 4, 8, 9$ systems are all in the chirally broken phase close to the continuum limit. Currently we are investigating $N_f = 9, 10, 11, 12$ on larger lattices to determine the lower edge of the conformal window. Lessons from the Dirac spectra and RMT to complement p-regime tests are discussed in the next section including comments about the controversial $N_f = 12$ case.

4. Epsilon regime, Dirac spectrum and RMT

If the bare parameters of a gauge theory are tuned to the ϵ -regime in the chirally broken phase, the low-lying Dirac spectrum follows the predictions of random matrix theory. The corresponding random matrix model is only sensitive to the pattern of chiral symmetry breaking, the topological charge and the rescaled fermion mass once the eigenvalues are also rescaled by the same factor $\Sigma_{cond}V$. This idea has been confirmed in various settings both in quenched and fully dynamical simulations. The same method is applied here to nearly conformal gauge models.

The connection between the eigenvalues λ of the Dirac operator and chiral symmetry breaking is given in the Banks-Casher relation [56],

$$\Sigma_{cond} = -\langle \bar{\Psi}\Psi \rangle = \lim_{\lambda \rightarrow 0} \lim_{m \rightarrow 0} \lim_{V \rightarrow \infty} \frac{\pi \rho(\lambda)}{V},$$

where Σ_{cond} designates the quark condensate normalized to a single flavor. To generate a non-zero density $\rho(0)$, the smallest eigenvalues must become densely packed as the volume increases, with an eigenvalue spacing $\Delta\lambda \approx 1/\rho(0) = \pi/(\Sigma_{cond}V)$. This allows a crude estimate of the quark condensate Σ_{cond} . One can do better by exploring the ϵ -regime: If chiral symmetry is spontaneously broken, tune the volume and quark mass such that $\frac{1}{F_\pi} \ll L \ll \frac{1}{M_\pi}$, so that the pion is much lighter than the physical value, and finite-volume effects are dominant as we discussed in Section 2. The chiral Lagrangian of Eq. (2) is dominated by the zero-momentum mode from the mass term and all kinetic terms are suppressed. In this limit, the distributions of the lowest eigenvalues are identical to those of random

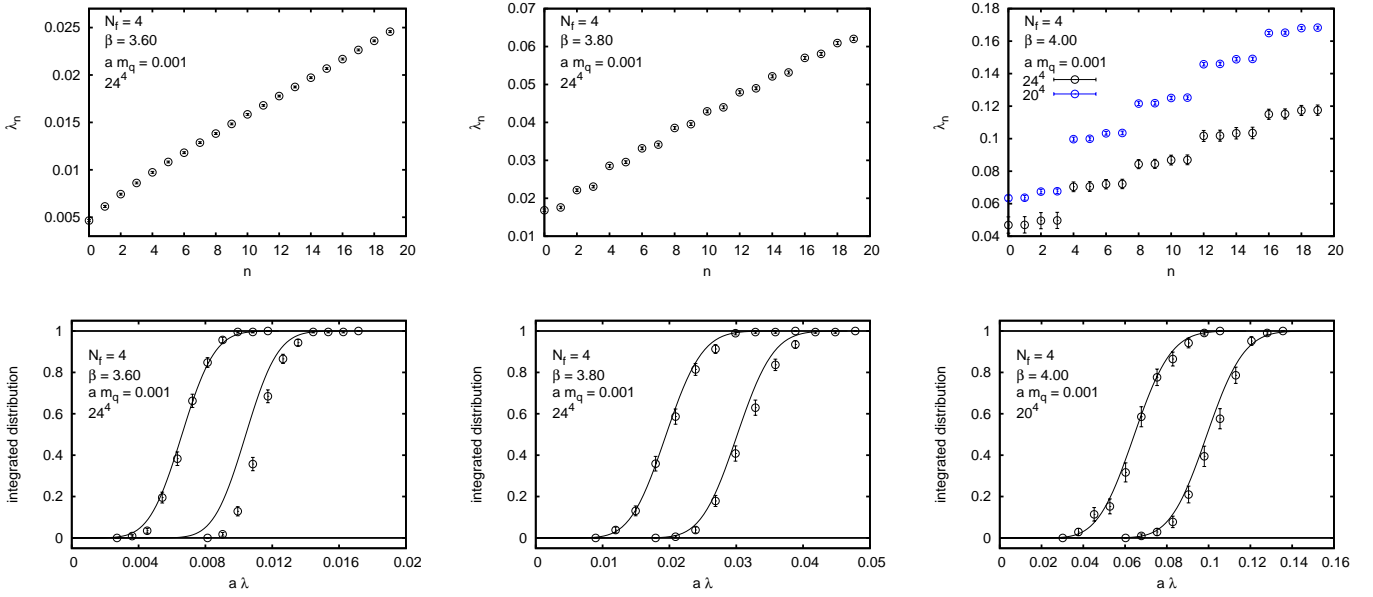


Figure 4: From simulations at $N_f = 4$ the first row shows the approach to quartet degeneracy of the spectrum as β increases. The second row shows the integrated distribution of the two lowest quartets averaged. The solid line compares this procedure to RMT with $N_f = 4$.

matrix theory, a theory of large matrices obeying certain symmetries [57, 58, 59]. To connect with RMT, the eigenvalues and quark mass are rescaled as $z = \lambda \Sigma_{cond} V$ and $\mu = m_q \Sigma_{cond} V$, and the eigenvalue distributions also depend on the topological charge ν and the number of quark flavors N_f . RMT is a very useful tool to calculate analytically all of the eigenvalue distributions. The eigenvalue distributions in various topological sectors are measured via lattice simulations, and via comparison with RMT, the value of the condensate Σ_{cond} can be extracted.

After we generate large thermalized ensembles, we calculate the lowest twenty eigenvalues of the Dirac operator using the PRIMME package [60]. In the continuum limit, the staggered eigenvalues form degenerate quartets, with restored taste symmetry. The first row of Fig. 4 shows the change in the eigenvalue structure for $N_f = 4$ as the coupling constant is varied. At $\beta = 3.6$ grouping into quartets is not seen, the pions are noticeably split, and staggered perturbation theory is just beginning to kick in. At $\beta = 3.8$ doublet pairing appears and at $\beta = 4.0$ the quartets are nearly degenerate. The Dirac spectrum is collapsed as required by the Banks-Casher relation. In the second row we show the integrated distributions of the two lowest eigenvalue quartet averages,

$$\int_0^\lambda p_k(\lambda') d\lambda', \quad k = 1, 2 \quad (15)$$

which is only justified close to quartet degeneracy. All low eigenvalues are selected with zero topology. To compare with RMT, we vary $\mu = m_q \Sigma_{cond} V$ until we satisfy

$$\frac{\langle \lambda_1 \rangle_{sim}}{m} = \frac{\langle z_1 \rangle_{RMT}}{\mu}, \quad (16)$$

where $\langle \lambda_1 \rangle_{sim}$ is the lowest quartet average from simulations and

the RMT average $\langle z \rangle_{RMT}$ depends implicitly on μ and N_f . With this optimal value of μ , we can predict the shapes of $p_k(\lambda)$ and their integrated distributions, and compare to the simulations. The agreement with the two lowest integrated RMT eigenvalue shapes is excellent for the larger β values.

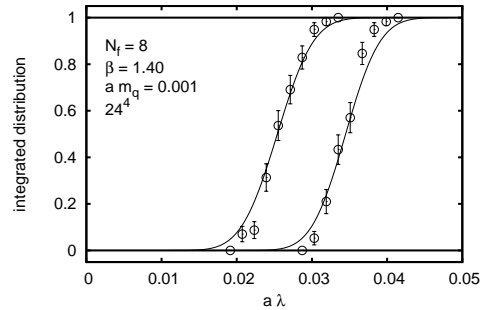


Figure 5: The solid lines compare the integrated distribution of the two lowest quartet averages to RMT predictions with $N_f = 8$.

The main qualitative features of the RMT spectrum are very similar in our $N_f = 8$ simulations as shown in Fig. 5. One marked quantitative difference is a noticeable slowdown in response to change in the coupling constant. As β grows the recovery of the quartet degeneracy is considerably delayed in comparison with the onset of p-regime Goldstone dynamics. Overall, for the $N_f = 4, 8$ models we find consistency between the p-regime analysis and the RMT tests. Earlier, using Asqtad fermions at a particular β value, we found agreement with RMT even at $N_f = 12$ which indicated a chirally broken phase [20]. Strong taste breaking with Asqtad fermion leaves the quartet averaging in question and the bulk pronounced crossover of the Asqtad action as β grows is also an issue. Currently we are investigating the RMT picture for $N_f = 9, 10, 11, 12$ with our

much improved action with four and six stout steps. This action shows no artifact transitions and handles taste breaking much more effectively. Firm conclusions on the $N_f = 12$ model will require continued investigations.

5. Inside the conformal window

We start our investigation and simulations of the conformal window at $N_f = 16$ which is the most accessible for analytic methods. We are particularly interested in the qualitative behavior of the finite volume spectrum of the model and the running coupling with its associated beta function which is expected to have a weak coupling fixed point around $g^{*2} \approx 0.5$, as estimated from the scheme independent two-loop beta function [61].

5.1. Conformal dynamics in finite volume

A distinguished feature of the $N_f = 16$ conformal model is how the renormalized coupling $g^2(L)$ runs with L , the linear size of the spatial volume in a Hamiltonian or Transfer Matrix description. On very small scales the running coupling $g^2(L)$ grows with L as in any other asymptotically free theory. However, $g^2(L)$ will not grow large, and in the $L \rightarrow \infty$ limit it will converge to the fixed point g^{*2} which is rather weak, within the reach of perturbation theory. There is nontrivial small volume dynamics which is illustrated first in the pure gauge sector.

At small g^2 , without fermions, the zero momentum components of the gauge field are known to dominate the dynamics [62, 63, 64]. With $SU(3)$ gauge group, there are twenty seven degenerate vacuum states, separated by energy barriers which are generated by the integrated effects of the non-zero momentum components of the gauge field in the Born-Oppenheimer approximation. The lowest energy excitations of the gauge field Hamiltonian scale as $\sim g^{2/3}(L)/L$ evolving into glueball states and becoming independent of the volume as the coupling constant grows with L . Nontrivial dynamics evolves through three stages as L grows. In the first regime, in very small boxes, tunneling is suppressed between vacua which remain isolated. In the second regime, for larger L , tunneling sets in and electric flux states will not be exponentially suppressed. Both regimes represent small worlds with zero momentum spectra separated from higher momentum modes of the theory with energies on the scale of $2\pi/L$. At large enough L the gauge dynamics overcomes the energy barrier, and wave functions spread over the vacuum valley. This third regime is the crossover to confinement where the electric fluxes collapse into thin string states wrapping around the box.

It is likely that a conformal theory with a weak coupling fixed point at $N_f = 16$ will have only the first two regimes which are common with QCD. Now the calculations have to include fermion loops [65, 66]. The vacuum structure in small enough volumes, for which the wave functional is sufficiently localized around the vacuum configuration, remains calculable by adding in one loop order the quantum effects of the fermion field fluctuations. The spatially constant abelian gauge fields parametrizing the vacuum valley are given by $A_i(\mathbf{x}) = T^a C_i^a/L$ where T_a are the $(N-1)$ generators for the Cartan subalgebra of $SU(N)$.

For $SU(3)$, $T_1 = \lambda_3/2$ and $T_2 = \lambda_8/2$. With N_f flavors of massless fermion fields the effective potential of the constant mode is given by

$$V_{\text{eff}}^{\mathbf{k}}(\mathbf{C}^b) = \sum_{i>j} V(\mathbf{C}^b[\mu_b^{(i)} - \mu_b^{(j)}]) - N_f \sum_i V(\mathbf{C}^b \mu_b^{(i)} + \pi \mathbf{k}), \quad (17)$$

with $\mathbf{k} = \mathbf{0}$ for periodic, or $\mathbf{k} = (1, 1, 1)$, for anti-periodic boundary conditions on the fermion fields. The function $V(\mathbf{C})$ is the one-loop effective potential for $N_f = 0$ and the weight vectors $\mu^{(i)}$ are determined by the eigenvalues of the abelian generators. For $SU(3)$ $\mu^{(1)} = (1, 1, -2)/\sqrt{12}$ and $\mu^{(2)} = \frac{1}{2}(1, -1, 0)$. The correct quantum vacuum is found at the minimum of this effective potential which is dramatically changed by the fermion loop contributions. The Polyakov loop observables re-

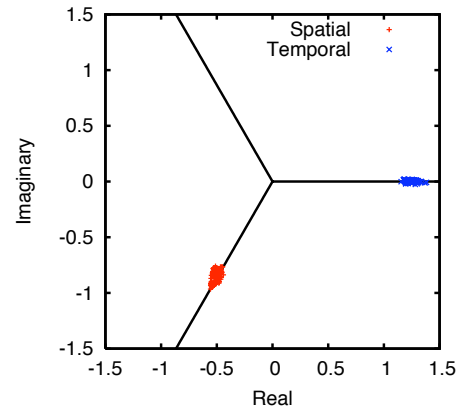


Figure 6: Polyakov loop distributions, blue in the time-like and red in the space-like directions, from our $N_f = 16$ simulation with 16^4 volume at $\beta = 18$ with tree level Symanzik improve gauge action and staggered fermions with six stout steps. The fermion boundary condition is anti-periodic in the time direction and periodic in the spatial directions.

main center elements at the new vacuum configurations with complex values

$$P_j = \frac{1}{N} \text{tr} \left(\exp(iC_j^b T_b) \right) = \frac{1}{N} \sum_n \exp(i\mu_b^{(n)} C_j^b) = \exp(2\pi i l_j / N), \quad (18)$$

for $SU(N)$. This implies that $\mu_b^{(n)} \mathbf{C}^b = 2\pi \mathbf{l} / N \pmod{2\pi}$, independent of n , and $V_{\text{eff}}^{\mathbf{k}} = -N_f N V(2\pi \mathbf{l} / N + \pi \mathbf{k})$. In the case of anti-periodic boundary conditions, $\mathbf{k} = (1, 1, 1)$, this is minimal only when $\mathbf{l} = \mathbf{0} \pmod{2\pi}$. The quantum vacuum in this case is the naive one, $A = 0$ ($P_j = 1$). In the case of periodic boundary conditions, $\mathbf{k} = \mathbf{0}$, the vacua have $\mathbf{l} \neq \mathbf{0}$, so that P_j correspond to non-trivial center elements. For $SU(3)$, there are now 8 degenerate vacua characterized by eight different Polyakov loops, $P_j = \exp(\pm 2\pi i / 3)$. Since they are related by coordinate reflections, in a small volume parity (P) and charge conjugation (C) are spontaneously broken, although CP is still a good symmetry [65]. As shown in Fig. 6, our simulations in the $N_f = 16$ model near the fixed point g^{*2} confirm this picture. In the weak coupling phase of the conformal window the time-like Polyakov loop takes the real root, while the space-like Polyakov loops always take the two other complex values, as expected on the basis of the above picture. Next we

will describe our method to probe the running coupling inside the conformal window. It is a pilot study for more comprehensive investigations of weak and strong coupling conformal dynamics.

5.2. Running coupling and beta function

Consider Wilson loops $W(R, T, L)$, where R and T are the space-like and time-like extents of the loop, and the lattice volume is L^4 (all dimensionful quantities are expressed in units of the lattice spacing a). A renormalized coupling can be defined by

$$g^2(R/L, L) = -\frac{R^2}{k(R/L)} \frac{\partial^2}{\partial R \partial T} \ln \langle W(R, T, L) \rangle |_{T=R}, \quad (19)$$

where for convenience the definition will be restricted to Wilson loops with $T = R$, and $\langle \dots \rangle$ is the expectation value of some quantity over the full path integral. This definition can be motivated by perturbation theory, where the leading term is simply the bare coupling g_0^2 . The renormalization scheme is defined by holding R/L to some fixed value. The quantity $k(R/L)$ is a geometric factor which can be determined by calculating the Wilson loop expectation values in lattice perturbation theory. The role of lattice simulations will be to measure non-perturbatively the expectation values. On the lattice, derivatives are replaced by finite differences, so the renormalized coupling is defined to be

$$g^2((R + 1/2)/L, L) = \frac{1}{k(R/L)} (R + 1/2)^2 \chi(R + 1/2, L),$$

$$\chi(R + 1/2, L) = -\ln \left[\frac{W(R + 1, T + 1, L) W(R, T, L)}{W(R + 1, T, L) W(R, T + 1, L)} \right] |_{T=R},$$

where χ is the Creutz ratio [67], and the renormalization scheme is defined by holding the value of $r = (R + 1/2)/L$ fixed.

With this definition, the renormalized coupling g^2 is a function of the lattice size L and the fixed value of r . The coupling is non-perturbatively defined, as the expectation values are calculated via lattice simulations, which integrate over the full phase space of the theory. By measuring $g^2(r, L)$ non-perturbatively for fixed r and various L values, the running of the renormalized coupling is mapped out. In a QCD-like theory, g^2 increases with increasing L as we flow in the infrared direction. In a conformal theory, g^2 flows towards some non-trivial infrared fixed point as L increases, whereas in a trivial theory, g^2 decreases with L . The advantage of this method is that no other energy scale is required to find the renormalization group flow. The renormalized coupling g^2 is also a function of the bare coupling g_0^2 , which is related to the lattice spacing a . Keeping the lattice spacing fixed, the running of $g^2(r, L)$ is affected by the lattice cut-off. The running has to be calculated in the continuum limit, extrapolating to zero lattice spacing. A similar method was developed independently in [68].

One way to measure the running of the renormalized coupling in the continuum limit is via step-scaling. The bare lattice coupling is defined in the usual way $\beta = 6/g_0^2$ as it appears in the lattice action. Some initial value of g^2 is picked from

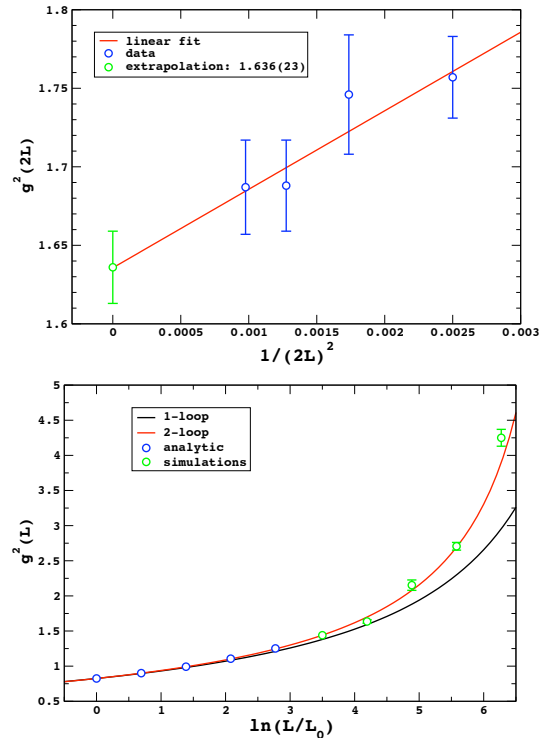


Figure 7: The method and the main test result for pure-gauge theory are shown in the figure. In the upper figure the extrapolation procedure picks up the leading a^2/L^2 cutoff correction term in the step function. It gives the fit to the continuum limit value of the step function. In the lower figure, the running coupling $g^2(L)$ is shown. The blue points are from results on Creutz ratios using analytic/numeric Wilson loop lattice calculations in finite volumes with fixed value of r . In this procedure we start from the one-loop expansion of Wilson loops in finite volumes based on the bare coupling [69]. The series is re-expanded in the boosted coupling constant at the relevant scale of the the Creutz ratio [70] to obtain realistic estimates of our running coupling without direct simulations. The rest of the procedure for the blue points follows what we described in the text. The green points are direct simulation results, following our procedure. The running starts at the point $g^2(L_0) = 0.825$. For almost all couplings there is excellent agreement with continuum 2-loop running. At the strongest coupling, the simulation results begin to break away from perturbation theory.

which the renormalization group flow is started. On a sequence of lattice sizes L_1, L_2, \dots, L_n , the bare coupling is tuned on each lattice so that exactly the same value $g^2(r, L_i, \beta_i)$ is measured from simulations. Now a new set of simulations is performed, on a sequence of lattice sizes $2L_1, 2L_2, \dots, 2L_n$, using the corresponding tuned couplings $\beta_1, \beta_2, \dots, \beta_n$. From the simulations, one measures $g^2(r, 2L_i, \beta_i)$, which will vary with the bare coupling *viz.* the lattice spacing. These data can be extrapolated to the continuum as a function of $1/L_i$. This gives one blocking step $L \rightarrow 2L$ in the continuum renormalization group flow. The whole procedure is then iterated. The chain of measurements gives the flow $g^2(r, L) \rightarrow g^2(r, 2L) \rightarrow g^2(r, 4L) \rightarrow g^2(r, 8L) \rightarrow \dots$, as far as is feasible (Fig. 7). One is free to choose a different blocking factor, say $L \rightarrow (3/2)L$, in which case more blocking steps are required to cover the same energy range.

We applied the above procedure to the running coupling in-

β	L	fermion mass	trajectories	$g^2(L)$
5	12	0.01	318	2.06(2)
	16	0.01	74	1.67(11)
7	12	0.01	317	1.207(5)
	12	0.001	116	1.207(12)
	16	0.01	198	1.13(1)
12	12	0.01	162	0.590(4)
	16	0.01	69	0.577(9)
15	12	0.01	144	0.447(3)
	12	0.001	91	0.460(5)
	16	0.01	62	0.444(7)
25	12	0.01	190	0.255(1)
	16	0.01	156	0.253(2)

Table 1: Running couplings bracketing the conformal fixed point of the $N_f = 16$ model in the conformal window.

side the conformal window with $N_f = 16$ flavors. The shortcut of this pilot study ignores the extrapolation to the continuum limit. The running coupling therefore is still contaminated with finite cutoff effects. If the linear lattice size L is large enough, the trend from the volume dependence of $g^2(L, a^2)$ should indicate the location of the fixed point. For $g^2(L, a^2) > g^{*2}$ we expect the decrease of the running coupling as L grows although the cutoff of the flow cannot be removed above the fixed point. Below the fixed point with $g^2(L, a^2) < g^{*2}$ we expect the running coupling to grow as L increases and the continuum limit of the flow could be determined. The first results are summarized in Table 1. They are consistent with the presented picture. For example, at bare couplings $\beta = 5, 7, 12$ the cutoff dependent renormalized coupling is larger than 0.5 and decreasing with growing L . At small bare couplings the renormalized coupling is flat within errors and the flow direction is not determined. The independence of the results from the small quark mass of the simulations is tested in two runs at $m_q = 0.001$. Precise determination of the conformal fixed point in the continuum requires further studies.

Acknowledgments

We are thankful to Claude Bernard and Steve Sharpe for help with staggered perturbation theory and to Ferenc Niedermayer for discussions on rotator dynamics. We also wish to thank Urs Heller for the use of his code to calculate Wilson loops in lattice perturbation theory, and Paul Mackenzie for related discussions. In some calculations we use the publicly available MILC code, and the simulations were performed on computing clusters at Fermilab, under the auspices of USQCD and SciDAC, on the Ranger cluster of the Teragrid organization, and on the Wuppertal GPU cluster. This work is supported by the NSF under grant 0704171, by the DOE under grants DOE-FG03-97ER40546, DOE-FG-02-97ER25308, by the DFG under grant FO 502/1 and by SFB-TR/55.

References

[1] S. Weinberg, Phys. Rev. D **19**, 1277 (1979).

- [2] L. Susskind, Phys. Rev. D **20**, 2619 (1979).
[3] E. Farhi and L. Susskind, Phys. Rept. **74**, 277 (1981).
[4] F. Sannino, arXiv:0902.3494 [hep-ph].
[5] T. A. Ryttov and F. Sannino, Phys. Rev. D **76**, 105004 (2007).
[6] D. D. Dietrich and F. Sannino, Phys. Rev. D **75**, 085018 (2007).
[7] D. K. Hong et al., Phys. Lett. B **597**, 89 (2004).
[8] H. Georgi, Phys. Rev. Lett. **98**, 221601 (2007).
[9] M. A. Luty and T. Okui, JHEP **0609**, 070 (2006).
[10] W. E. Caswell, Phys. Rev. Lett. **33**, 244 (1974).
[11] T. Banks and A. Zaks, Nucl. Phys. B **196**, 189 (1982).
[12] T. Appelquist et al., Phys. Rev. Lett. **61**, 1553 (1988).
[13] A. G. Cohen and H. Georgi, Nucl. Phys. B **314**, 7 (1989).
[14] T. Appelquist et al., Phys. Rev. Lett. **77**, 1214 (1996).
[15] B. Holdom, Phys. Rev. D **24**, 1441 (1981).
[16] K. Yamawaki et al., Phys. Rev. Lett. **56**, 1335 (1986).
[17] T. W. Appelquist et al., Phys. Rev. Lett. **57**, 957 (1986).
[18] V. A. Miransky and K. Yamawaki, Phys. Rev. D **55**, 5051 (1997).
[19] E. Eichten and K. D. Lane, Phys. Lett. B **90**, 125 (1980).
[20] Z. Fodor et al., PoS **LATTICE2008**, 066 (2008)
[21] Z. Fodor et al., PoS **LATTICE2008**, 058 (2008)
[22] Z. Fodor et al., arXiv:0905.3586 [hep-lat].
[23] T. DeGrand et al., Phys. Rev. D **79**, 034501 (2009).
[24] T. DeGrand et al., arXiv:0809.2953 [hep-lat].
[25] B. Svetitsky et al., arXiv:0809.2885 [hep-lat].
[26] Y. Shamir et al., Phys. Rev. D **78**, 031502 (2008).
[27] T. Appelquist et al., arXiv:0901.3766 [hep-ph].
[28] T. Appelquist et al., Phys. Rev. Lett. **100**, 171607 (2008)
[29] G. T. Fleming, PoS **LATTICE2008**, 021 (2008)
[30] L. Del Debbio et al., arXiv:0812.0570 [hep-lat].
[31] L. Del Debbio et al., arXiv:0805.2058 [hep-lat].
[32] L. Del Debbio et al., JHEP **0806**, 007 (2008)
[33] A. J. Hietanen et al., arXiv:0904.0864 [hep-lat].
[34] A. J. Hietanen et al., arXiv:0812.1467 [hep-lat].
[35] A. Hietanen et al., PoS **LATTICE2008**, 065 (2008)
[36] A. Deuzeman et al., arXiv:0904.4662 [hep-ph].
[37] A. Deuzeman et al., arXiv:0810.3117 [hep-lat].
[38] A. Deuzeman et al., PoS **LATTICE2008**, 060 (2008)
[39] A. Deuzeman et al., Phys. Lett. B **670**, 41 (2008)
[40] S. Catterall and F. Sannino, Phys. Rev. D **76**, 034504 (2007)
[41] S. Catterall et al., JHEP **0811**, 009 (2008)
[42] X. Y. Jin and R. D. Mawhinney, PoS **LATTICE2008**, 059 (2008)
[43] A. Hasenfratz, arXiv:0907.0919 [hep-lat].
[44] T. DeGrand and A. Hasenfratz, arXiv:0906.1976 [hep-lat].
[45] T. DeGrand, arXiv:0906.4543 [hep-lat].
[46] L. Del Debbio et al., arXiv:0907.3896 [hep-lat].
[47] C. Morningstar and M. J. Peardon, Phys. Rev. D **69**, 054501 (2004)
[48] W. J. Lee and S. R. Sharpe, Phys. Rev. D **60**, 114503 (1999)
[49] C. Aubin and C. Bernard, Phys. Rev. D **68**, 034014 (2003)
[50] C. Aubin and C. Bernard, Phys. Rev. D **68**, 074011 (2003)
[51] J. Gasser and H. Leutwyler, Nucl. Phys. B **307**, 763 (1988).
[52] F. C. Hansen and H. Leutwyler, Nucl. Phys. B **350**, 201 (1991).
[53] J. Gasser and H. Leutwyler, Annals Phys. **158**, 142 (1984).
[54] M. Gell-Mann et al., Phys. Rev. **175**, 2195 (1968).
[55] H. Leutwyler, Phys. Lett. B **189**, 197 (1987).
[56] T. Banks and A. Casher, Nucl. Phys. B **169**, 103 (1980).
[57] E. V. Shuryak and J. J. M. Verbaarschot, Nucl. Phys. A **560**, 306 (1993)
[58] P. H. Damgaard, Nucl. Phys. Proc. Suppl. **128**, 47 (2004)
[59] J. J. M. Verbaarschot and T. Wettig, Ann. Rev. Nucl. Part. Sci. **50**, 343 (2000)
[60] A. Stathopoulos and J. R. McCombs, SIAM J. Sci. Comput., Vol. **29**, No. **5**, 2162 (2007).
[61] U. M. Heller, Nucl. Phys. Proc. Suppl. **63**, 248 (1998)
[62] G. 't Hooft, Nucl. Phys. B **153**, 141 (1979).
[63] M. Luscher, Nucl. Phys. B **219**, 233 (1983).
[64] P. van Baal and J. Koller, Annals Phys. **174**, 299 (1987).
[65] P. van Baal, Nucl. Phys. B **307**, 274 (1988).
[66] J. Kripfganz and C. Michael, Nucl. Phys. B **314**, 25 (1989).
[67] M. Creutz, Phys. Rev. D **21**, 2308 (1980).
[68] E. Bilgici et al., arXiv:0902.3768 [hep-lat].
[69] U. M. Heller and F. Karsch, Nucl. Phys. B **251**, 254 (1985).
[70] G. P. Lepage and P. B. Mackenzie, Phys. Rev. D **48**, 2250 (1993)